remote sensing

MDPI

Communication

Assessment of CALIOP-Derived CCN Concentrations by In Situ Surface Measurements

Goutam Choudhury * and Matthias Tesche

Leipzig Institute for Meteorology, Leipzig University, 04103 Leipzig, Germany; matthias.tesche@uni-leipzig.de
* Correspondence: goutam.choudhury@uni-leipzig.de

Abstract: The satellite-based cloud condensation nuclei (CCN) proxies used to quantify the aerosol-cloud interactions (ACIs) are column integrated and do not guarantee the vertical co-location of aerosols and clouds. This has encouraged the use of height-resolved measurements of spaceborne lidars for ACI studies and led to advancements in lidar-based CCN retrieval algorithms. In this study, we present a comparison between the number concentration of CCN (n_{CCN}) derived from ground-based in situ and spaceborne lidar cloud-aerosol lidar with orthogonal polarization (CALIOP) measurements. On analysing their monthly time series, we found that about 88% of CALIOP n_{CCN} estimates remained within a factor of 1.5 of the in situ measurements. Overall, the CALIOP estimates of monthly n_{CCN} were in good agreement with the in situ measurements with a normalized mean error of 71%, normalized mean bias of 39% and correlation coefficient of 0.68. Based on our comparison results, we point out the necessary measures that should be considered for global n_{CCN} retrieval. Our results show the competence of CALIOP in compiling a global height- and type-resolved n_{CCN} dataset for use in ACI studies.

Keywords: CCN validation; CALIPSO validation; OMCAM; POLIPHON; aerosol-cloud interactions

check for updates

Citation: Choudhury, G.; Tesche, M. Assessment of CALIOP-Derived CCN Concentrations by In Situ Surface Measurements. *Remote Sens.* **2022**, *14*, 3342. https://doi.org/10.3390/rs14143342

Academic Editor: Carmine Serio

Received: 7 June 2022
Accepted: 10 July 2022
Published: 11 July 2022

Publisher's Note: MDPI stays neutral with regard to jurisdictional claims in published maps and institutional affiliations.

1. Introduction

Aerosol particles form an important component of Earth's radiative budget by either interacting directly with short- and longwave radiation, or indirectly by acting as cloud condensation nuclei (CCN), which affect cloud properties. Under most atmospheric conditions, aerosols are required for water vapor to condense into cloud droplets. Thus, changes in aerosol concentration may alter the number of cloud droplets formed within a cloud [1] and adjust the cloud's extent and lifetime [2]. These aerosol-cloud interactions (ACIs) are the major contributor to the total aerosol effective radiative forcing and still remain the most uncertain component of anthropogenic radiative forcing [3].

The impact of changes in aerosol concentration on cloud droplets is non-linear. It depends not only on the aerosol's physical (size and shape) and chemical properties (hygroscopicity) but also on ambient meteorological parameters such as water vapor content and atmospheric stability [4–6]. The aerosol concentration may vary regionally by several orders of magnitude (10 to 10^5 cm^{-3}) depending on the type, strength, and proximity of sources and sinks. Today, in situ aerosol observatories provide continuous and temporally highly resolved long-term measurements of cloud-relevant aerosol properties such as aerosol-sized distribution and chemical composition and CCN concentrations at different supersaturations (ss). However, they are limited to selected geographical locations. In contrast, satellite instruments can provide global observations of aerosols and clouds and, thus, are used extensively for studying ACIs with constrained meteorology and selected cloud regimes [7–9].

The fundamental aerosol information needed to study ACIs for liquid clouds is the number of available CCN close to the cloud base as only those will interact with the cloud droplets. Satellite retrievals, however, give aerosol optical properties, which are

used either directly as proxies for the number concentration of CCN (n_{CCN}) or to derive information on the cloud-relevant aerosol fraction. Most satellite-based ACI studies use aerosol optical depth (AOD) [10–12] or an aerosol index (AI) [13–16] as CCN proxies. The AOD may not be an accurate proxy for CCN as it does not include any information about the size of the observed aerosol particles. For instance, a large number of small particles can result in the same AOD as a small number of large particles. Furthermore, hydrophobic particles that are less efficient CCN compared to hygroscopic particles may contribute significantly to the AOD. Conversely, the AI, as the product of the AOD, and the Ångström exponent form a slightly better qualitative CCN proxy than the AOD as it is weighted more towards fine aerosols [17,18]. To better quantify the radiative forcing associated with ACI, Hasekamp et al. [19] used polarimetric observations over oceans to infer column-integrated, aerosol-sized distributions. They further used the aerosol number concentration with a wet radius >150 nm as the CCN proxy and found the forcing estimates to be almost 50% higher than those where the AOD or AI were used. One of the intrinsic limitations of using any of the three CCN proxies is that they are all column-integrated parameters, i.e., they may not necessarily represent aerosols close to the cloud base, which are the ones relevant for ACI [20,21]. Moreover, the AI and polarimetric retrievals are not reliable over land [18,22], where most of the anthropogenic aerosols are generated and the concentrations are the highest. A way to overcome the shortcomings associated with CCN products inferred from observations with passive sensors is to shift towards height-resolved aerosol and cloud observations using spaceborne lidar, which is available over both land and ocean [18].

Shinozuka et al. [23] used in situ measurements to report a linear relation between n_{CCN} and the aerosol extinction coefficient on a log–log scale. Following their work, Mamouri and Ansmann [24] present the first CCN retrieval algorithm for ground-based lidar, where specific aerosol-type extinction-to-number-concentration conversion factors are used to infer the number concentration of particles larger than a set radius. This particle concentration is subsequently used in CCN parametrizations to estimate n_{CCN} at multiple supersaturations. The application to spaceborne Cloud-Aerosol Lidar with Orthogonal Polarization (CALIOP) observations was found to give aerosol number concentrations that were in reasonable agreement with in situ measurements [25–27]. In a recent study, Choudhury and Tesche [28] presented a CCN retrieval algorithm that had been developed specifically for CALIOP application. The algorithm used normalized size distributions in the CALIOP aerosol model [29] and scaled them to reproduce the CALIOP-derived extinction coefficient. These inferred aerosol-type specific-size distributions were integrated to obtain aerosol number concentrations that were found to be in reasonable agreement with airborne in situ measurements [27]. However, a direct comparison of CALIOP-derived CCN concentrations with in situ CCN measurements is still missing in the validation of both algorithms.

Schmale et al. [30] presented multi-year continuous co-located in situ measurements of n_{CCN} and aerosol size distributions at 11 ground stations that covered a variety of environments with varying aerosol signatures. Here, we compare the n_{CCN} estimated from spaceborne CALIOP data using the aforementioned methodologies with the ground-based in situ measurements of Schmale et al. [30]. The concurrent in situ measurements of n_{CCN} and aerosol-sized distribution were furthermore used to assess the applicability of CCN parameterizations related to different aerosol types and size ranges. Based on our results, we also suggest necessary measures for compiling a global CCN climatology. The article is structured as follows. We describe the datasets, retrieval algorithms, and comparison methodology in Section 2. The comparison between the in situ and satellite derived n_{CCN} is given in Section 3. The findings and possible steps forward are summarized in the final section.

2. Data and Methods

2.1. In Situ Observations

The in situ observations used in this study were obtained from Schmale et al. [30]. The dataset consists of simultaneous measurements of aerosol-sized distributions and n_{CCN} at multiple supersaturations for 11 ground-based stations. The data have a temporal resolution of one hour and include a total of 98,677 h and 157,880 h of n_{CCN} and size distribution measurements, respectively. Of the 11 stations, we used measurements from 7 stations: Barrow, Cabauw, Finokalia, Melpitz, Vavihill, Puy de Dôme, and Seoul. Station selection was based on the availability, location, and proximity of the CALIOP overpasses relative to the station location. Other factors, such as very low aerosol concentrations (Mace Head) and presence of clouds (Jungfraujoch) close to the surface, hindered CALIOP retrievals; thus, such stations were not considered in our comparison. Among the selected stations, Puy de Dôme is a high-altitude station that represents the continental background and free-tropospheric air masses. Barrow and Finokalia are coastal stations covering Arctic and Mediterranean conditions. Cabauw, Melpitz, and Vavihill represent continental background conditions, while Seoul characterizes the polluted urban environment. The geographical location of these stations is shown in Figure 1. Details about the altitude, environment, and temporal coverage of each site are listed in Table 1. A comprehensive description of the instruments, inlet system, sampling procedure, and quality control measures used in the data collection at each station is given in Schmale et al. [30].

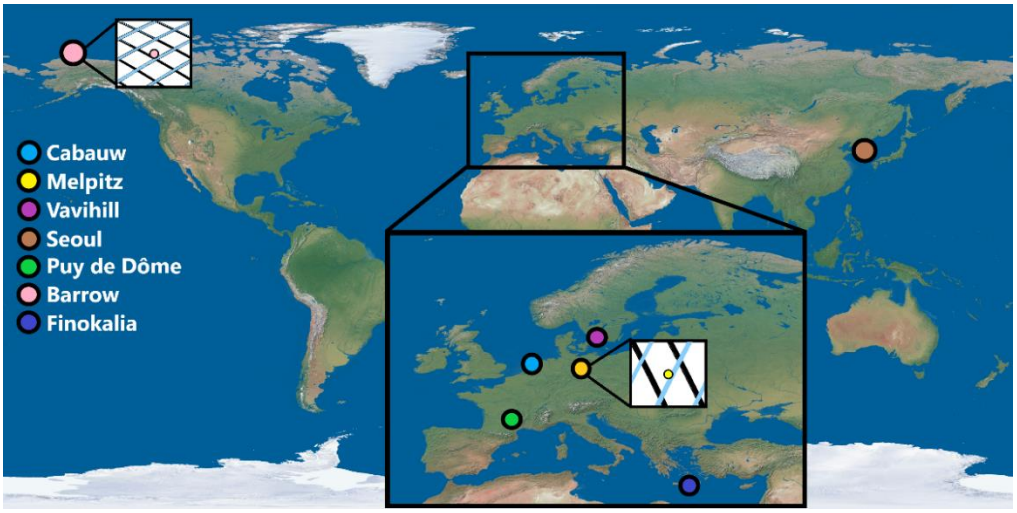

Figure 1. Location of the in situ sites used in this study. The large inset gives a closer look of Europe. The small insets present daytime (blue) and nighttime (black) ground tracks of CALIOP that fall within a 3° × 3° latitude–longitude grid box centered at Melpitz and Barrow, respectively, for a randomly selected month. The world map in the background is taken from http://www.shadedrelief.com/natural3/pages/textures.html (accessed on 7 July 2022).

Table 1. Details of the in situ stations considered in this study.

Station	Environment	Location	Elevation	Temporal Coverage
Cabauw, The Netherlands	near coast, continental background	51°58′N, 4°56′E	−1 m	1 January 2012–31 December 2014
Melpitz, Germany	continental background	51°32′N, 12°56′E	86 m	1 January 2012–31 December 2014
Vavihill, Sweden	rural background	56°01′N, 13°09′E	172 m	20 December 2012–11 November 2014
Seoul, South Korea	urban, monsoon-influenced	37°34′N 126°58′E	38 m	1 January 2006–31 December 2010

Table 1. *Cont.*

Station	Environment	Location	Elevation	Temporal Coverage
Puy de Dôme, France	mountain, continental background	45°46′N, 02°57′E	1465 m	1 January 2014–1 January 2015
Barrow, USA	Arctic maritime	71°19′N, 156°37′W	11 m	20 July 2007–25 June 2008
Finokalia, Greece	coastal background, Mediterranean	35°20′N, 25°40′E	250 m	1 January 2014–31 December 2015

2.2. CALIOP

CALIOP is a two-wavelength polarization-sensitive lidar on the Cloud-Aerosol Lidar and Infrared Pathfinder Satellite Observations (CALIPSO) satellite, which has been observing the vertical distribution and occurrence of aerosols and clouds since June 2006 [31]. CALIPSO aerosol products include vertical profiles of the aerosol extinction coefficient, aerosol backscatter coefficient, particle–linear depolarization ratio, and aerosol subtype. CALIPSO aerosol subtypes defined in the most recent version 4 data products include marine, dust, dusty marine, polluted dust, clean continental, polluted continental/smoke, and elevated smoke [32]. In the present work, we used the CALIPSO level 2 version 4.20 aerosol profile product [33], which included aerosol optical properties and subtype information at a uniform horizontal resolution of 5 km and a vertical resolution of 60 m within the troposphere. We also used the relative humidity profiles included in the CALIPSO product obtained from the Global Modelling and Assimilation Office Data Assimilation System [34].

CCN Concentrations from CALIOP

The Optical Modelling of CALIPSO Aerosol Microphysics (OMCAM) [28] and the Polarization Lidar Photometer Networking (POLIPHON) [24,35] are the two techniques for estimating CCN concentrations from CALIOP measurements. Prior to the application of the CALIPSO aerosol parameters, we applied all the quality control measures suggested by Tackett et al. [36] and only selected high-quality cloud-free retrievals. We also separated the dust mixtures into dust and non-dust contributions following Tesche et al. [37]. In both methods, we first needed to convert the CALIOP extinction coefficient to dry number concentrations of aerosols within a size range where they were likely to act as CCN. The number concentration was then used in aerosol-type specific CCN parametrizations to compute n_{CCN} at defined supersaturations. POLIPHON uses a set of equations to convert the CALIOP extinction coefficient (α) to a dry aerosol number concentration with radius greater than j nm ($n_{j,dry}$) as

$$n_{j,dry} = C\ \alpha^{x}, \quad (1)$$

where j is 50 nm for continental and marine aerosols and 100 nm for dust aerosols; C is the conversion factor; and x is the extinction exponent obtained from the regression analysis of long-term AERONET measurements of AOD and size distributions [24,38,39]. The values of C and x used in this work are listed in Table 2. Similar to Choudhury et al. [27], we used regression constants for continental (clean continental and polluted continental) and marine aerosols from Mamouri and Ansmann [24], desert dust from Ansmann et al. [38], and smoke aerosols from Ansmann et al. [39].

In contrast to POLIPHON, OMCAM uses the aerosol microphysical properties (normalized size distributions and refractive indices) in the CALIPSO aerosol model [29] and scales the size distribution to reproduce the CALIOP extinction coefficient [28] using the MOPSMAP modelling package [40]. The scaled size distribution is then used to compute the required aerosol number concentration to be used in the corresponding CCN parametrization. While evaluating the OMCAM estimated aerosol number concentrations with airborne in situ measurements, Choudhury et al. [27] found that the marine model

from Omar et al. [29] resulted in an underestimation of $n_{50,dry}$ and suggested using the AERONET-based marine model from Sayer et al. [41]. We thus used the OMCAM algorithm with an updated marine model in our validation study. To correct the ambient CALIOP extinction coefficient for the hygroscopicity of hydrophilic aerosols, we used the kappa parametrization [42] included in the MOPSMAP package with globally averaged kappa values of 0.3 for continental aerosols (clean continental, polluted continental, elevated smoke), and 0.7 for marine aerosols [43]. Schmale et al. [44] also found similar kappa values using the in situ data considered in this study. Dust is treated as hydrophobic, so no hygroscopicity correction was applied for dust retrievals. To apply the hygroscopicity correction, following Choudhury et al. [27], we first estimated the growth factors at different relative humidity (RH) values for different aerosol subtypes using the microphysical properties from the CALIPSO aerosol model and Sayer et al. [41] (for marine subtype). We then correct the CALIOP extinction coefficient by using these growth factors. Previous studies found this method to yield reasonable results even under highly humid conditions such as within the marine boundary layer [27,28]. Choudhury et al. [27] parametrized the dry aerosol number concentrations linearly (x = 1 in Equation (1)) for the dry aerosol extinction coefficient. The corresponding values are given in Table 2. It is worth noting that the linear relationship in OMCAM held only for the dry extinction coefficient. In contrast, the POLIPHON technique was originally formulated for ambient conditions assuming a constant RH of 80 and 60% for marine and continental aerosols, respectively [24]. Thus, for POLIPHON, we only applied the hygroscopicity correction when the ambient RH exceeded these values for the corresponding aerosol types.

Table 2. Conversion factor (C in Mm cm^{-3}) and extinction exponent (x) values for POLIPHON and OMCAM algorithms used to estimate $n_{j,dry}$ from Equation (1). Note that x = 1 for OMCAM.

Type	POLIPHON (Ambient)		OMCAM (Dry)
	C	x	C
Dust	8.855	0.7525	11.085
Clean continental	25.3	0.94	3.6
Marine	7.2	0.85	2.4
Elevated smoke	17	0.79	22
Polluted continental	25.3	0.94	24.93

The fraction of aerosols that can act as CCN depends not only on the particles' physical and chemical properties but also on the atmospheric water vapor supersaturation, depends on meteorological parameters such as temperature, pressure, water content, vertical wind velocity and the resulting cooling rate. Given the complexities in measuring atmospheric n_{CCN}, Mamouri and Ansmann [24] defined $n_{j,dry}$ in Equation (1) as representing the n_{CCN} at ss = 0.15–0.20%. The n_{CCN} at higher supersaturations are expressed as a multiple of $n_{j,dry}$. In the present work, we considered CALIOP-derived n_{CCN} at ss = 0.2% (i.e., $n_{j,dry}$) in the comparison study because this parameter was provided by all of the in situ stations. The in situ data included simultaneous measurements of hourly n_{CCN} and aerosol-sized distributions [30]. To assess the CCN parameterizations used in our retrievals, we compared the $n_{j,dry}$ as estimated from the size distributions with measurements of the n_{CCN} at 0.2% supersaturation. Figure 2 shows a comparison of the in situ n_{CCN} from direct measurements and $n_{j,dry}$ inferred from the concurrent in situ size-distribution measurements for the sites listed in Table 1. We considered $n_{50,dry}$ for all stations except Finokalia, for which we compared $n_{100,dry}$ as this particular site is frequently influenced by dust aerosols [30,44]. This approach was also supported by the CALIOP profiles within a 3° by 3° grid box surrounding the station in which 70–90% of the monthly extinction coefficients were classified as related to dust, polluted dust, and dusty marine aerosol subtypes (not shown).

Figure 2 shows very good agreement between in situ $n_{j,\mathrm{dry}}$ and n_{CCN} with a Spearman correlation coefficient (R) of 0.9, a normalized mean bias (NMB) of 20%, and normalized mean error (NME) of 34%. We therefore concluded that the use of aerosol-size-based CCN parametrizations as suggested by Mamouri and Ansmann [24] provided reasonable estimates of n_{CCN}.

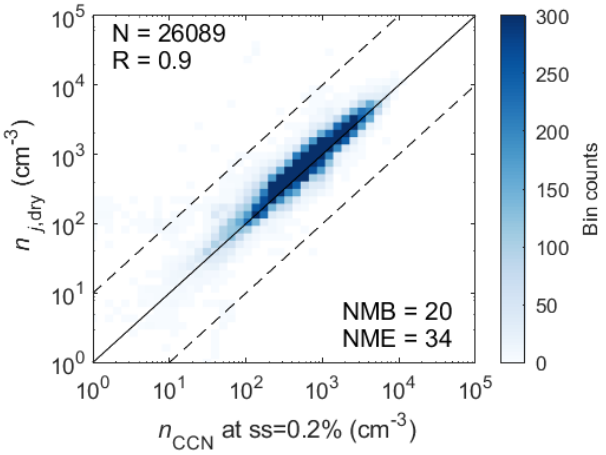

Figure 2. Comparison of concurrent in situ measurements of hourly n_{CCN} at 0.2% supersaturation and $n_{j,\mathrm{dry}}$ (j = 100 nm for dust influenced Finokalia station and j = 50 nm for other sites). The values of correlation coefficient (R), total number of bins (N), normalized mean bias (NMB) and normalized mean error (NME) are given in the legend.

2.3. Comparison Methodology

Compared to passive sensors and the resulting column-integrated parameters, CALIOP measures height-resolved aerosol properties that can be aggregated to obtain their spatial and vertical distribution. However, CALIOP has a very small footprint on the order of tens of meters compared to the hundreds of kilometers of passive sensors. Hence, monthly CALIPSO level 3 data products are reported at a coarse 2° × 5° latitude–longitude grid [36,45]. To compare CALIOP observations with those at the in situ stations considered in this study, we defined a 3° × 3° latitude–longitude grid box centered at the geographical location of a station and then considered all the CALIPSO level 2 profiles within that domain. Thus, the selected profiles were used to compute the n_{CCN} as discussed in Section 2.2. These individual profiles were then averaged to obtain monthly mean profiles of n_{CCN} for each grid box that was compared to the in situ data. Monthly averaging was used to compensate for (i) the relatively large area in the satellite-to-surface comparison that might include scenarios in which CALIOP and an in situ site observed different air masses and (ii) the local extremes in the in situ time series that were unlikely to be covered in the satellite observations. Note that our grid was finer than the 5° × 5° in Fanourgakis et al. [46] for comparing multi-model simulations of n_{CCN} with surface in situ measurements. For comparison to the in situ data at ground, CALIOP-derived profiles of CCN concentration were averaged from the surface to 1 km in height (to capture boundary-layer aerosols) except for the alpine site (Puy de Dôme), for which the averaging was extended to a height of 2 km. The comparison method used to determine the absolute error between the satellite and in situ measurement was the NME and to assess the relative bias of the satellite retrieval it was the NMB. The Spearman correlation coefficient (R) was used to assess the ability of satellite retrievals to represent the variability in the in situ measurements. As the CALIOP-derived n_{CCN} represented $n_{j,\mathrm{dry}}$ (j = 50 nm for continental and marine, and 100 nm for dust aerosols) at 0.2% supersaturation, we also compared them with the in situ measurements of $n_{j,\mathrm{dry}}$ (j = 100 nm for dust influenced Finokalia station and 50 nm for other stations). This approach enabled us to consider in situ measurements also for months that were lacking CCN measurements and to increases the number of data points to be considered in the statistical analysis.

3. Comparison of CCN Concentrations

The comparison of the monthly mean n_{CCN} (at ss = 0.2%) at the in situ stations and inferred from CALIOP measurements is presented in Figure 3 and Table 3. At all sites, monthly in situ $n_{j,dry}$ are either comparable or larger than the directly measured in situ n_{CCN} with average NMB and NME values of 20.7 and 39.8%, respectively and nearly identical monthly variations. Overall, the CALIOP estimates of monthly n_{CCN} using OMCAM algorithm were larger than the in situ observations with a mean NMB and NME of 49% (31%) and 76% (93%) for nighttime (daytime) retrievals, respectively. The POLIPHON algorithm resulted in even larger CCN values with NMB and NME values of 129% (89%) and 138.5% (133.2%) for nighttime (daytime) retrievals, respectively. A fraction of this overestimation comes from the consideration of pure size-based CCN parameterization (Equation (1)), which considers all aerosols within the selected size limit to be CCN active. This is also seen in Figures 2 and 3, where $n_{j,dry}$ overestimated n_{CCN} with a positive bias of about 20%. The statistics improve somewhat for the comparison of $n_{j,dry}$ (Table 3). The best n_{CCN} absolute error agreement was found at Puy de Dôme with nighttime OMCAM estimates resulting in an absolute error of about 43%. Overall, worst agreement between CALIOP and in situ measurements was found at dust-influenced Finokalia with NME values as high as a factor of 1 for OMCAM and 1.5 for POLIPHON retrievals. Such disagreement was also reported in Choudhury et al. [27] for dust and marine aerosol mixtures and may be because of changes in the microphysical properties of the aerosol types caused by either chemical or cloud processing. Assuming dust aerosols to be hydrophobic may also have contributed to the disagreement. Overall, about 88% (91%) and 77% (88%) of either of the daytime or nighttime monthly CALIOP n_{CCN} estimates from OMCAM and POLIPHON algorithms, respectively, stayed within a factor of 1.5 of the monthly in situ n_{CCN} ($n_{j,dry}$) measurements. In some cases, the findings from CALIOP daytime and nighttime retrievals differed by several orders of magnitude. On closer inspection, we found that the daytime and nighttime tracks covered different geographical locations within a grid box. Furthermore, in any given month, the number of days with a daytime CALIPSO track within the considered domain was not always the same as that for nighttime overpasses. Also, the sensitivity of CALIOP to aerosols was different during day and night. These factors were likely to have caused the differences observed between the daytime and nighttime n_{CCN} retrievals.

Table 3. Comparison statistics of monthly n_{CCN} at ss = 0.2% (in cm^{-3}) and $n_{j,dry}$ (in cm^{-3}) derived from in situ and CALIOP measurements. The values enclosed within brackets are for daytime CALIOP retrievals and the unbracketed values represent nighttime retrievals. The normalized mean bias (NMB) and normalized mean error (NME) are given along with their averages weighted by the number of observation months for each station.

Stations	NMB (%)				NME (%)			
	OMCAM		POLIPHON		OMCAM		POLIPHON	
	n_{CCN}	$n_{j,dry}$	n_{CCN}	$n_{j,dry}$	n_{CCN}	$n_{j,dry}$	n_{CCN}	$n_{j,dry}$
Cabauw	44 (−9.9)	14.2 (−30.3)	123.3 (36.7)	79.8 (6.13)	72 (53.2)	66.6 (40.6)	134.8.1 (84.6)	102.6 (47.7)
Melpitz	47 (7.8)	43 (53.1)	134.9 (62.5)	128.5 (135)	82.7 (70)	78 (97.8)	151.6 (104.6)	140.3 (154.1)
Vavihill	17 (54.3)	12.1 (33.7)	99.6 (147.6)	83.6 (115)	44.2 (82.2)	47.8 (66.5)	105.4 (159.2)	92.1 (129)
Seoul	31.5 (19.6)	2.7 (−10.6)	88.3 (62.9)	48.9 (23.5)	75.3 (80)	39.7 (49)	106.5 (97.9)	63.5 (59)
Puy de Dôme	29.5 (100.8)	23.5 (122.2)	125.7 (219.2)	115.2 (254.6)	43 (157.3)	41.4 (172.3)	125.7 (254.1)	115.2 (281.1)
Barrow	113.6 (−41.7)	1 (−15)	241.7 (−15.7)	61.6 (56.7)	117.5 (84.9)	72.5 (55.8)	241.7 (94.2)	80.7 (70.9)
Finokalia	93.9 (127.3)	109.8 (126.3)	151.9 (146.1)	167.8 (150)	106.8 (189.3)	109.8 (170.4)	154.7 (196)	167.8 (174.1)
Average	48.8 (31.1)	26.7 (25.3)	128.6 (89)	91.2 (78.4)	75.9 (93.3)	62.6 (79.4)	138.5 (133.2)	104.3 (107.9)

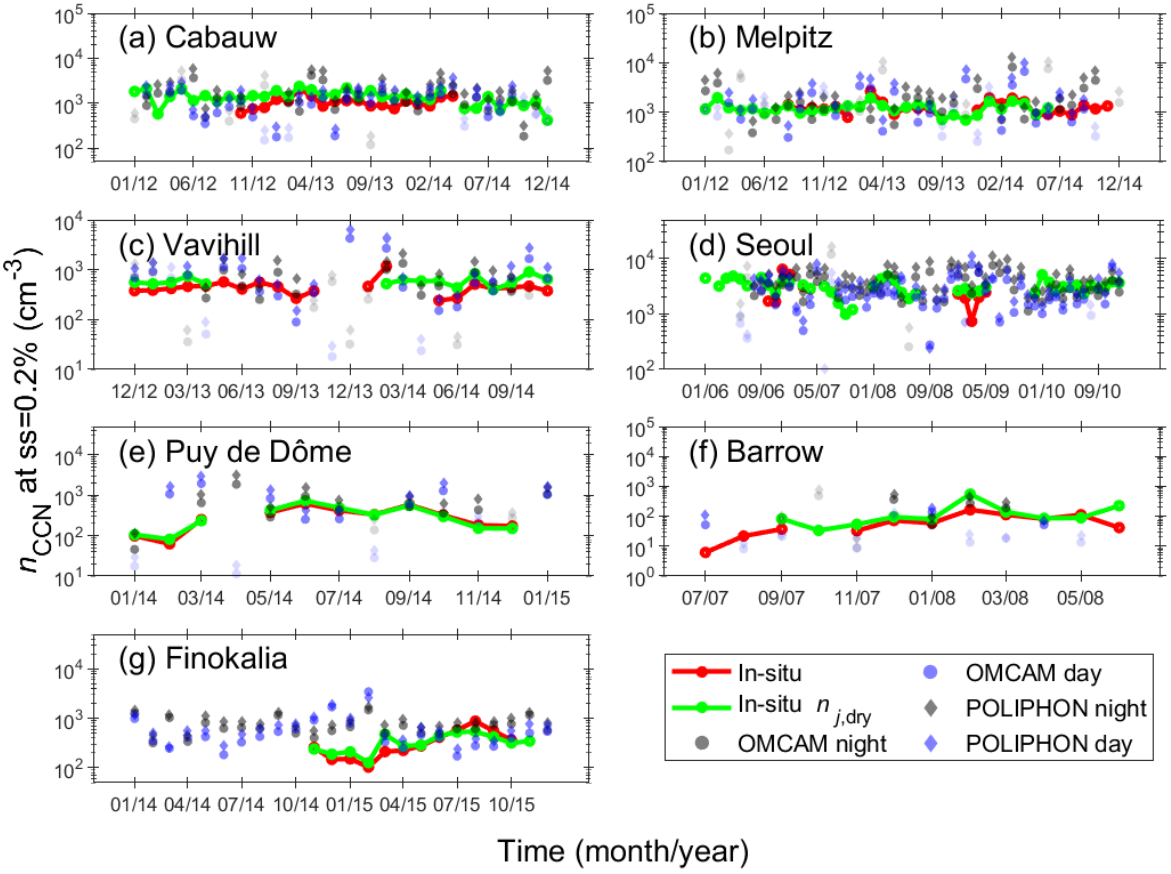

Figure 3. Monthly time series of $n_{j,\mathrm{dry}}$ (green) and n_{CCN} (red) as derived from ground-based in situ measurements and n_{CCN} inferred from CALIOP observations using the OMCAM (gray dots for nighttime data and blue for daytime data) and POLIPHON (gray diamonds for nighttime and blue for daytime data) algorithms at Cawbauw (**a**), Melpitz (**b**), Vavihill (**c**), Seoul (**d**), Puy de Dôme (**e**), Barrow (**f**), and Finokalia (**g**) stations. The semi-transparent data points are for the cases where the number of CALIOP data bins with finite aerosol retrievals used to produce the monthly average are less than 100.

It is known that CALIOP may fail to detect aerosol layers with a lower aerosol load [18,47,48]. On analyzing the number of CALIOP data bins with valid aerosol retrieval (N_{bins}) used to compute the monthly n_{CCN} time series in Figure 3, we identified several cases where $N_{bins} < 100$ (25th percentile) coincided with outliers (semi-transparent points in Figure 3). Figure 4 shows how the comparison of CALIOP-derived CCN concentrations with the in situ measurements improved when only months with $N_{bins} > 100$ are considered in the analysis. In that case, the CALIOP estimates of n_{CCN} using POLIPHON are in reasonable agreement with the in situ $n_{j,\mathrm{dry}}$ and n_{CCN} with NME values of 83 and 123%, NMB values of 62 and 108%, and R values of 0.61 and 0.7, respectively. The OMCAM estimates were in even better agreement with the in situ $n_{j,\mathrm{dry}}$ and n_{CCN} with NME values of 54 and 71%, NMB values of 9 and 39%, and R values of 0.63 and 0.68, respectively.

Along with the aerosol load, the number of days in a month observed (DMO) by CALIOP within a grid box may also have a significant impact on the n_{CCN} retrieval. In general, CALIOP-derived monthly values are expected to be more representative of a region within higher DMO. The DMO value depends on the geographical location (about 19 days at high latitude Barrow and 7 days at Melpitz station) and the size of the grid box, especially along the longitude. As the former cannot be modulated, increasing the grid box for CALIOP sampling is the only possible way to get higher DMO values. We therefore suggest using a relatively coarse $2^\circ \times 5^\circ$ latitude–longitude grid (also used in CALIPSO level 3 data [36]) to estimate a global height-resolved n_{CCN} to obtain a regionally representative

result. Even so, CALIOP has the potential to provide height- and type-resolved n_{CCN} over both land and oceans. With regards to the ACI study, the height-resolved measurements can be used to estimate the n_{CCN} close to cloud base and the type-resolved measurements to quantify the anthropogenic component. The availability of more than a decade of CALIOP measurements provides a unique opportunity to study the global and seasonal distribution of CCN concentrations for different aerosol types. However, such a study is not within the scope of the present work and will be presented in future studies.

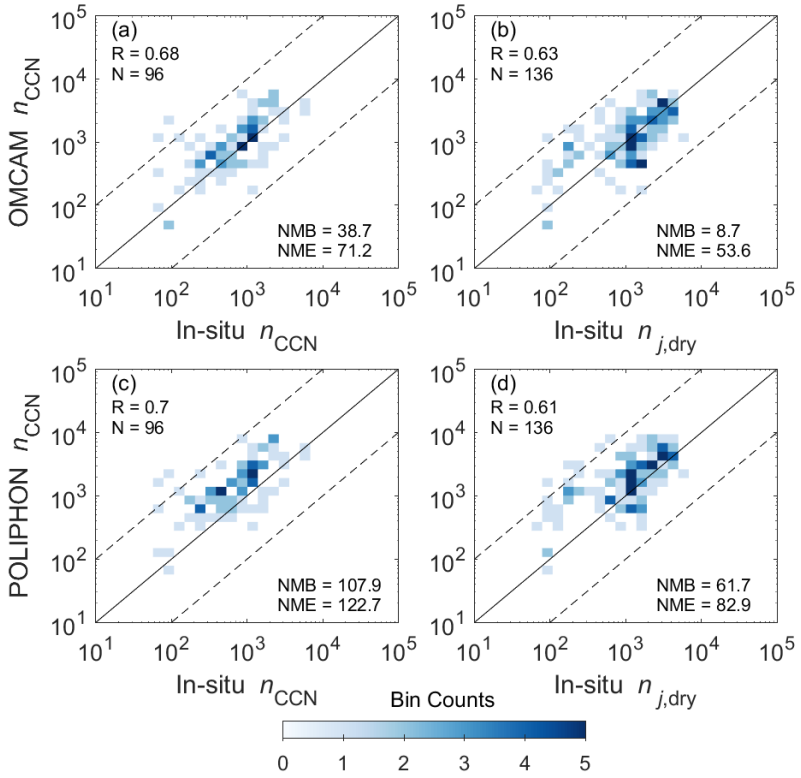

Figure 4. Comparison of n_{CCN} (**a**,**c**) and $n_{j,dry}$ (**b**,**d**) from in situ and CALIOP (day and night combined) measurements using OMCAM (**a**,**b**) and POLIPHON (**c**,**d**) for $N_{bins} > 100$ at all sites given in Table 1.

4. Conclusions

We presented a comparison of monthly in situ CCN concentrations (n_{CCN}) and dry aerosol number concentrations ($n_{j,dry}$) with the spaceborne lidar CALIOP retrievals. POLIPHON and OMCAM algorithms were used to estimate $n_{j,dry}$ and n_{CCN} from CALIOP measurements. Both techniques rely on size-based CCN parametrizations. A comparison of the concurrent in situ measurements of n_{CCN} and $n_{j,dry}$ at all stations supported the applicability of the size-based CCN parametrizations. We found that the CALIOP estimates of monthly n_{CCN} at 0.2% supersaturation were generally in good agreement with the in situ measurements: about 88% (91%) and 77% (88%) of n_{CCN} ($n_{j,dry}$) estimates from OMCAM and POLIPHON algorithms remaining within a factor of 1.5 of the in situ measurements, respectively. Disagreement was primarily found for the monthly retrievals where the number of aerosol samples detected by CALIOP was less than 100 (25th percentile). Excluding such retrievals, we found the OMCAM n_{CCN} estimates to have better agreement with the in situ measurements with a normalized mean error of 71%, normalized mean bias of 39%, and correlation coefficient of 0.68.

The in situ stations considered in this validation study cover different continental environments. Future studies involving a direct comparison of CALIOP retrievals with measurements over oceans, (e.g., from Hudson et al. [49]) will provide better insight into the ability of CALIOP to estimate marine n_{CCN}. Having said that, our findings along

with previous comparison studies [25–28] support the feasibility of constructing a global height-resolved n_{CCN} climatology from CALIOP measurements. Such a dataset would be invaluable not only for studying aerosol-cloud interactions [8,18] but also serve as a benchmark for regional and global climate models.

Author Contributions: G.C. conceptualized the study, performed the data analysis, and prepared the plots under the guidance of M.T., G.C. prepared the initial version of the paper. G.C. and M.T. contributed to the discussion of the findings and the revisions of the paper. All authors have read and agreed to the published version of the manuscript.

Funding: This research has been supported by the Franco-German Fellowship Program on Climate, Energy, and Earth System Research (Make Our Planet Great Again—German Research Initiative (MOPGA–GRI), grant number 57429422) of the German Academic Exchange Service (DAAD), funded by the German Ministry of Education and Research.

Data Availability Statement: The CALIPSO level 2 v4.20 aerosol profile data product used in this work is available at https://doi.org/10.5067/CALIOP/CALIPSO/LID_L2_05KMAPRO-STANDARD-V4-20 (accessed on 7 July 2022). The in situ data is available at http://actris.nilu.no/Content/products (accessed on 7 July 2022).

Acknowledgments: We thank the CALIPSO science team for providing the CALIPSO data and the AERIS/ICARE Data and Services Center for providing access to the data used in this study. We are thankful to the PI's, technical, and non-technical members involved in the collection and management of the in situ dataset used in our study.

Conflicts of Interest: The authors declare no conflict of interest.

References

1. Twomey, S. Pollution and the planetary albedo. *Atmos. Environ.* **1974**, *8*, 1251–1256. [CrossRef]
2. Albrecht, B.A. Aerosols, Cloud Microphysics, and Fractional Cloudiness. *Science* **1989**, *245*, 1227–1230. [CrossRef] [PubMed]
3. Forster, P.; Storelvmo, T.; Armour, K.; Collins, W.; Dufresne, J.-L.; Frame, D.; Lunt, D.J.; Mauritsen, T.; Palmer, M.D.; Watanabe, M.; et al. The Earth's Energy Budget, Climate Feedbacks, and Climate Sensitivity. In *Climate Change 2021: The Physical Science Basis. Contribution of Working Group I to the Sixth Assessment Report of the Intergovernmental Panel on Climate Change*; Masson-Delmotte, V., Zhai, P., Pirani, A., Connors, S.L., Péan, C., Berger, S., Caud, N., Chen, Y., Goldfarb, L., Gomis, M.I., et al., Eds.; Cambridge University Press: Cambridge, UK, 2021.
4. Fan, J.; Wang, Y.; Rosenfeld, D.; Liu, X. Review of Aerosol–Cloud Interactions: Mechanisms, Significance, and Challenges. *J. Atmos. Sci.* **2016**, *73*, 4221–4252. [CrossRef]
5. Seinfeld, J.H.; Bretherton, C.; Carslaw, K.S.; Coe, H.; DeMott, P.J.; Dunlea, E.J.; Feingold, G.; Ghan, S.; Guenther, A.B.; Kahn, R.; et al. Improving our fundamental understanding of the role of aerosol−cloud interactions in the climate system. *Proc. Natl. Acad. Sci. USA* **2016**, *113*, 5781–5790. [CrossRef] [PubMed]
6. Choudhury, G.; Tyagi, B.; Singh, J.; Sarangi, C.; Tripathi, S. Aerosol-orography-precipitation—A critical assessment. *Atmos. Environ.* **2019**, *214*, 116831. [CrossRef]
7. Oreopoulos, L.; Cho, N.; Lee, N. Using MODIS Cloud Regimes to Sort Diagnostic Signals of Aerosol-Cloud-Precipitation Interactions. *J. Geophys. Res. Atmos.* **2017**, *122*, 5416–5440. [CrossRef]
8. Bellouin, N.; Quaas, J.; Gryspeerdt, E.; Kinne, S.; Stier, P.; Watson-Parris, D.; Boucher, O.; Carslaw, K.S.; Christensen, M.; Daniau, A.; et al. Bounding Global Aerosol Radiative Forcing of Climate Change. *Rev. Geophys.* **2020**, *58*, e2019RG000660. [CrossRef]
9. Douglas, A.; L'Ecuyer, T. Quantifying variations in shortwave aerosol–cloud–radiation interactions using local meteorology and cloud state constraints. *Atmos. Chem. Phys.* **2019**, *19*, 6251–6268. [CrossRef]
10. Feingold, G.; Remer, L.A.; Ramaprasad, J.; Kaufman, Y.J. Analysis of smoke impact on clouds in Brazilian biomass burning regions: An extension of Twomey's approach. *J. Geophys. Res. Earth Surf.* **2001**, *106*, 22907–22922. [CrossRef]
11. Quaas, J.; Boucher, O.; Bellouin, N.; Kinne, S. Satellite-based estimate of the direct and indirect aerosol climate forcing. *J. Geophys. Res. Earth Surf.* **2008**, *113*, D05204. [CrossRef]
12. Quaas, J.; Ming, Y.; Menon, S.; Takemura, T.; Wang, M.; Penner, J.E.; Gettelman, A.; Lohmann, U.; Bellouin, N.; Boucher, O.; et al. Aerosol indirect effects—General circulation model intercomparison and evaluation with satellite data. *Atmos. Chem. Phys.* **2009**, *9*, 8697–8717. [CrossRef]
13. Nakajima, T.; Higurashi, A.; Kawamoto, K.; Penner, J.E. A possible correlation between satellite-derived cloud and aerosol microphysical parameters. *Geophys. Res. Lett.* **2001**, *28*, 1171–1174. [CrossRef]
14. Bréon, F.-M.; Tanré, D.; Generoso, S. Aerosol Effect on Cloud Droplet Size Monitored from Satellite. *Science* **2002**, *295*, 834–838. [CrossRef] [PubMed]

15. Lohmann, U.; Lesins, G. Stronger Constraints on the Anthropogenic Indirect Aerosol Effect. *Science* **2002**, *298*, 1012–1015. [CrossRef]
16. Gryspeerdt, E.; Quaas, J.; Ferrachat, S.; Gettelman, A.; Ghan, S.; Lohmann, U.; Morrison, H.; Neubauer, D.; Partridge, D.G.; Stier, P.; et al. Constraining the instantaneous aerosol influence on cloud albedo. *Proc. Natl. Acad. Sci. USA* **2017**, *114*, 4899–4904. [CrossRef] [PubMed]
17. Stier, P. Limitations of passive remote sensing to constrain global cloud condensation nuclei. *Atmos. Chem. Phys.* **2016**, *16*, 6595–6607. [CrossRef]
18. Quaas, J.; Arola, A.; Cairns, B.; Christensen, M.; Deneke, H.; Ekman, A.M.L.; Feingold, G.; Fridlind, A.; Gryspeerdt, E.; Hasekamp, O.; et al. Constraining the Twomey effect from satellite observations: Issues and perspectives. *Atmos. Chem. Phys.* **2020**, *20*, 15079–15099. [CrossRef]
19. Hasekamp, O.P.; Gryspeerdt, E.; Quaas, J. Analysis of polarimetric satellite measurements suggests stronger cooling due to aerosol-cloud interactions. *Nat. Commun.* **2019**, *10*, 5405. [CrossRef]
20. Costantino, L.; Bréon, F.-M. Analysis of aerosol-cloud interaction from multi-sensor satellite observations. *Geophys. Res. Lett.* **2010**, *37*, L11801. [CrossRef]
21. Costantino, L.; Bréon, F.-M. Aerosol indirect effect on warm clouds over South-East Atlantic, from co-located MODIS and CALIPSO observations. *Atmos. Chem. Phys.* **2013**, *13*, 69–88. [CrossRef]
22. Sayer, A.M.; Hsu, N.C.; Bettenhausen, C.; Jeong, M.J. Validation and uncertainty estimates for MODIS Collection 6 "Deep Blue" aerosol data. *J. Geophys. Res. Atmos.* **2013**, *118*, 7864–7872. [CrossRef]
23. Shinozuka, Y.; Clarke, A.D.; Nenes, A.; Jefferson, A.; Wood, R.; McNaughton, C.S.; Ström, J.; Tunved, P.; Redemann, J.; Thornhill, K.L.; et al. The relationship between cloud condensation nuclei (CCN) concentration and light extinction of dried particles: Indications of underlying aerosol processes and implications for satellite-based CCN estimates. *Atmos. Chem. Phys.* **2015**, *15*, 7585–7604. [CrossRef]
24. Mamouri, R.-E.; Ansmann, A. Potential of polarization lidar to provide profiles of CCN- and INP-relevant aerosol parameters. *Atmos. Chem. Phys.* **2016**, *16*, 5905–5931. [CrossRef]
25. Marinou, E.; Tesche, M.; Nenes, A.; Ansmann, A.; Schrod, J.; Mamali, D.; Tsekeri, A.; Pikridas, M.; Baars, H.; Engelmann, R.; et al. Retrieval of ice-nucleating particle concentrations from lidar observations and comparison with UAV in situ measurements. *Atmos. Chem. Phys.* **2019**, *19*, 11315–11342. [CrossRef]
26. Georgoulias, A.K.; Marinou, E.; Tsekeri, A.; Proestakis, E.; Akritidis, D.; Alexandri, G.; Zanis, P.; Balis, D.; Marenco, F.; Tesche, M.; et al. A First Case Study of CCN Concentrations from Spaceborne Lidar Observations. *Remote Sens.* **2020**, *12*, 1557. [CrossRef]
27. Choudhury, G.; Ansmann, A.; Tesche, M. Evaluation of aerosol number concentrations from CALIPSO with ATom airborne in situ measurements. *Atmos. Chem. Phys.* **2022**, *22*, 7143–7161. [CrossRef]
28. Choudhury, G.; Tesche, M. Estimating cloud condensation nuclei concentrations from CALIPSO lidar measurements. *Atmos. Meas. Tech.* **2022**, *15*, 639–654. [CrossRef]
29. Omar, A.H.; Winker, D.M.; Vaughan, M.A.; Hu, Y.; Trepte, C.R.; Ferrare, R.A.; Lee, K.-P.; Hostetler, C.A.; Kittaka, C.; Rogers, R.R.; et al. The CALIPSO Automated Aerosol Classification and Lidar Ratio Selection Algorithm. *J. Atmos. Ocean. Technol.* **2009**, *26*, 1994–2014. [CrossRef]
30. Schmale, J.; Henning, S.; Henzing, B.; Keskinen, H.; Sellegri, K.; Ovadnevaite, J.; Bougiatioti, A.; Kalivitis, N.; Stavroulas, I.; Jefferson, A.; et al. Collocated observations of cloud condensation nuclei, particle size distributions, and chemical composition. *Sci. Data* **2017**, *4*, 170003. [CrossRef]
31. Winker, D.M.; Vaughan, M.A.; Omar, A.; Hu, Y.; Powell, K.A.; Liu, Z.; Hunt, W.H.; Young, S. Overview of the CALIPSO Mission and CALIOP Data Processing Algorithms. *J. Atmos. Ocean. Technol.* **2009**, *26*, 2310–2323. [CrossRef]
32. Kim, M.-H.; Omar, A.H.; Tackett, J.L.; Vaughan, M.A.; Winker, D.M.; Trepte, C.R.; Hu, Y.; Liu, Z.; Poole, L.R.; Pitts, M.C.; et al. The CALIPSO version 4 automated aerosol classification and lidar ratio selection algorithm. *Atmos. Meas. Tech.* **2018**, *11*, 6107–6135. [CrossRef] [PubMed]
33. *NASA/LARC/SD/ASDC CALIPSO Lidar Level 2 Aerosol Profile, V4-20 [Data Set]*; NASA Langley Atmospheric Science Data Center DAAC, 2018. Available online: https://doi.org/10.5067/CALIOP/CALIPSO/LID_L2_05KMAPRO-STANDARD-V4-20 (accessed on 7 July 2022).
34. Molod, A.; Takacs, L.; Suarez, M.; Bacmeister, J. Development of the GEOS-5 atmospheric general circulation model: Evolution from MERRA to MERRA2. *Geosci. Model Dev.* **2015**, *8*, 1339–1356. [CrossRef]
35. Mamouri, R.E.; Ansmann, A. Estimated desert-dust ice nuclei profiles from polarization lidar: Methodology and case studies. *Atmos. Chem. Phys.* **2015**, *15*, 3463–3477. [CrossRef]
36. Tackett, J.L.; Winker, D.M.; Getzewich, B.J.; Vaughan, M.A.; Young, S.A.; Kar, J. CALIPSO lidar level 3 aerosol profile product: Version 3 algorithm design. *Atmos. Meas. Tech.* **2018**, *11*, 4129–4152. [CrossRef] [PubMed]
37. Tesche, M.; Ansmann, A.; Mueller, D.; Althausen, D.; Engelmann, R.; Freudenthaler, V.; Gross, S. Vertically resolved separation of dust and smoke over Cape Verde using multiwavelength Raman and polarization lidars during Saharan Mineral Dust Experiment 2008. *J. Geophys. Res. Space Phys.* **2009**, *114*, D13202. [CrossRef]
38. Ansmann, A.; Mamouri, R.-E.; Hofer, J.; Baars, H.; Althausen, D.; Abdullaev, S.F. Dust mass, cloud condensation nuclei, and ice-nucleating particle profiling with polarization lidar: Updated POLIPHON conversion factors from global AERONET analysis. *Atmos. Meas. Tech.* **2019**, *12*, 4849–4865. [CrossRef]

39. Ansmann, A.; Ohneiser, K.; Mamouri, R.-E.; Knopf, D.A.; Veselovskii, I.; Baars, H.; Engelmann, R.; Foth, A.; Jimenez, C.; Seifert, P.; et al. Tropospheric and stratospheric wildfire smoke profiling with lidar: Mass, surface area, CCN, and INP retrieval. *Atmos. Chem. Phys.* **2021**, *21*, 9779–9807. [CrossRef]
40. Gasteiger, J.; Wiegner, M. MOPSMAP v1.0: A versatile tool for the modeling of aerosol optical properties. *Geosci. Model Dev.* **2018**, *11*, 2739–2762. [CrossRef]
41. Sayer, A.M.; Smirnov, A.; Hsu, N.C.; Holben, B.N. A pure marine aerosol model, for use in remote sensing applications. *J. Geophys. Res. Earth Surf.* **2012**, *117*, D05213. [CrossRef]
42. Petters, M.D.; Kreidenweis, S.M. A single parameter representation of hygroscopic growth and cloud condensation nucleus activity. *Atmos. Chem. Phys.* **2007**, *7*, 1961–1971. [CrossRef]
43. Andreae, M.; Rosenfeld, D. Aerosol–cloud–precipitation interactions. Part 1. The nature and sources of cloud-active aerosols. *Earth-Sci. Rev.* **2008**, *89*, 13–41. [CrossRef]
44. Schmale, J.; Henning, S.; Decesari, S.; Henzing, B.; Keskinen, H.; Sellegri, K.; Ovadnevaite, J.; Pöhlker, M.L.; Brito, J.; Bougiatioti, A.; et al. Long-term cloud condensation nuclei number concentration, particle number size distribution and chemical composition measurements at regionally representative observatories. *Atmos. Chem. Phys.* **2018**, *18*, 2853–2881. [CrossRef]
45. Winker, D.M.; Tackett, J.L.; Getzewich, B.J.; Liu, Z.; Vaughan, M.A.; Rogers, R.R. The global 3-D distribution of tropospheric aerosols as characterized by CALIOP. *Atmos. Chem. Phys.* **2013**, *13*, 3345–3361. [CrossRef]
46. Fanourgakis, G.S.; Kanakidou, M.; Nenes, A.; Bauer, S.E.; Bergman, T.; Carslaw, K.S.; Grini, A.; Hamilton, D.S.; Johnson, J.S.; Karydis, V.A.; et al. Evaluation of global simulations of aerosol particle and cloud condensation nuclei number, with implications for cloud droplet formation. *Atmos. Chem. Phys.* **2019**, *19*, 8591–8617. [CrossRef]
47. Watson-Parris, D.; Schutgens, N.; Winker, D.; Burton, S.P.; Ferrare, R.A.; Stier, P. On the Limits of CALIOP for Constraining Modeled Free Tropospheric Aerosol. *Geophys. Res. Lett.* **2018**, *45*, 9260–9266. [CrossRef]
48. Ma, P.-L.; Rasch, P.J.; Chepfer, H.; Winker, D.M.; Ghan, S.J. Observational constraint on cloud susceptibility weakened by aerosol retrieval limitations. *Nat. Commun.* **2018**, *9*, 2640. [CrossRef]
49. Hudson, J.G.; Noble, S.; Jha, V. Stratus Cloud Supersaturations. *Geophys. Res. Lett.* **2010**, *37*, L21813. [CrossRef]